

Guided Skyrmion Motion Along Pinning Array Interfaces

N. P. Vizarim^{a,b}, C. Reichhardt^a, P. A. Venegas^c, C. J. O. Reichhardt^a

^a*Theoretical Division and Center for Nonlinear Studies, Los Alamos National Laboratory, Los Alamos, New Mexico 87545, USA*

^b*POSMAT - Programa de Pós-Graduação em Ciência e Tecnologia de Materiais, Faculdade de Ciências, Universidade Estadual Paulista - UNESP, Bauru, SP, CP 473, 17033-360, Brazil*

^c*Departamento de Física, Faculdade de Ciências, Universidade Estadual Paulista - UNESP, Bauru, SP, CP 473, 17033-360, Brazil*

Abstract

We examine ac driven skyrmions interacting with the interface between two different obstacle array structures. We consider drive amplitudes at which skyrmions in a bulk obstacle lattice undergo only localized motion and show that when an obstacle lattice interface is introduced, directed skyrmion transport can occur along the interface. The skyrmions can be guided by a straight interface and can also turn corners to follow the interface. For a square obstacle lattice embedded in a square pinning array with a larger lattice constant, we find that skyrmions can undergo transport in all four primary symmetry directions under the same fixed ac drive. We map where localized or translating motion occurs as a function of the ac driving parameters. Our results suggest a new method for controlling skyrmion motion based on transport along obstacle lattice interfaces.

Keywords: Skyrmion, Ratchet effects, Edge transport

1. Introduction

Skyrmions are particlelike magnetic textures that are stabilized by their topological properties [1–3]. They have attracted growing interest as an increasing number of materials have been identified in which skyrmions are stable over an extended range of parameters, including at room temperature [4–10]. Skyrmions also have interesting basic science properties as a representative example of an emergent phenomenon in which the microscopic degrees of freedom in the form of spins act collectively to form particle-like objects which in turn experience competing interactions with temperature, disorder, other skyrmions, and coupling to external drives. Due to their size, stability, and ability to be manipulated with external drives, skyrmions are also very promising for applications such as magnetic based memory and logic devices [11]. There have been a number of proposals on how to create different types of devices for moving

skyrmions that interact with some form of nanostructured sample or pinning array [9, 12–16].

One of the properties of skyrmions that makes them distinct from many other particlelike systems interacting with a substrate is that skyrmions have a strong gyroscopic component to their motion in the form of a Magnus force [3, 17, 18]. The Magnus force generates a velocity component that is perpendicular to the net force on the skyrmion, and tends to produce spiraling motion in the presence of localized defects as well as a skyrmion Hall effect in which the skyrmion moves at an angle with respect to an external drive [3, 17–21]. When a moving skyrmion interacts with a pinning site or barrier, the Magnus force can strongly affect the skyrmion motion, resulting in a drive dependence of the skyrmion Hall angle [19–26], as well as acceleration effects or skyrmion deflection [27–30].

For skyrmions interacting with a periodic array of pinning sites or obstacles under a dc drive, the skyrmion Hall angle is not constant but increases with increasing skyrmion velocity and exhibits a series of steps produced when the skyrmion motion locks to symmetry directions of the substrate, followed by a saturation at high velocities to the intrinsic or disorder free value [31–33]. When combined ac and dc driving is used to move skyrmions over a periodic pinning array, a variety of both directional locking and phase locking effects appear [34, 35]. The phase locking effects resemble Shapiro steps in which the ac drive frequency matches with the intrinsic frequency of the motion of the skyrmion over the periodic substrate, leading to steps in the skyrmion velocity-force curves [36, 37]. The Magnus force can generate additional features in the Shapiro steps that are not found in overdamped systems such as superconducting vortices moving over two-dimensional (2D) periodic pinning under dc and ac driving [38, 39].

Under purely ac driving, skyrmions interacting with a 2D periodic substrate can pass through a series of localized and delocalized orbits as the size of the orbit increases [40]. In the localized orbits, the skyrmion encircles or moves through an integer number of pinning sites. For ac parameters which place the skyrmion orbit at the boundary between two different stable commensurate orbits, the motion is chaotic and the skyrmion diffuses through the system. It is even possible in some cases to obtain directed skyrmion motion under purely ac driving by using a biharmonic or circular ac drive to induce a ratchet effect [34, 40]. In studies of skyrmions interacting with periodic obstacle arrays, the directed motion has a fixed orientation if the ac drive amplitude and frequency is held fixed [40]. For potential device applications, it would be valuable to be able to steer the skyrmions along a specified trajectory involving arbitrary directions using only a single applied ac drive.

Here we demonstrate that steerable skyrmion motion can be achieved with a single ac drive in a system where the skyrmions interact with an interface between two different periodic obstacle arrays, as illustrated in Fig. 1. We specifically show that the skyrmion can move along the interface and turn corners, allowing controlled motion of the skyrmion in all four lattice symmetry directions. The motion along the interface is quantized, and a single interface can produce different modes of motion as the ac drive parameters are varied.

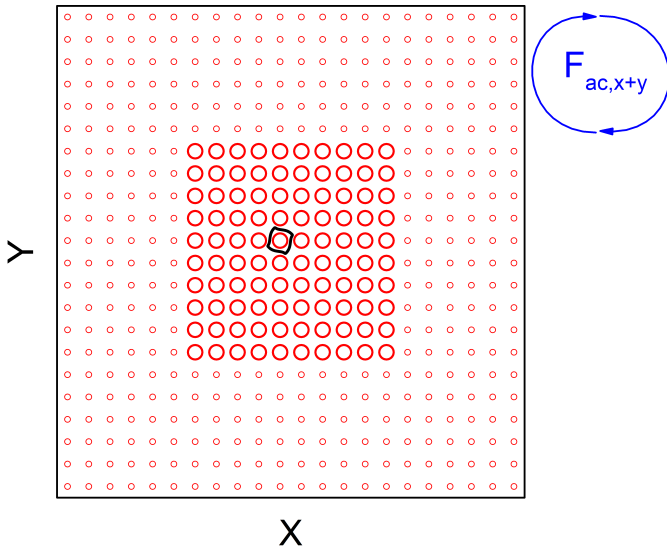


Figure 1: Image of a system containing a square array of larger obstacles (large circles) with radius $R_o^L = 0.85$ set inside a square array of smaller obstacles (small circles) with radius $R_o^S = 0.45$. Both arrays have the same lattice constant. The black line indicates a trajectory of a skyrmion trapped in the larger obstacle array under a circular ac drive $F_{ac,x+y}$.

In some cases the skyrmion remains locked along the interface and follows the edges, while in other cases the skyrmion can travel along a single straight interface but decouples from the interface upon reaching a corner. The skyrmion motion we observe is similar to the edge transport phenomenon found in colloidal topological insulators [41], where particle transport can occur along the interface between two different substrate geometries. Our results show that skyrmion edge transport can be realized and that it represents a new method for controlling and steering skyrmion motion to create new types of devices.

2. Simulation

We consider a 2D system with periodic boundary conditions in the x and y directions. The sample contains two periodic arrays of obstacles with identical lattice constant a but varied obstacle radii R_o^L (for the large obstacles) and R_o^S (for the small obstacles). We introduce a single skyrmion near the interface edge or in the bulk and drive it with a circular ac force. The skyrmion dynamics is modeled using the modified Thiele equation approach as in previous work [19, 26, 31, 33], where the equation of motion for the skyrmion is:

$$\alpha_d \mathbf{v}_i + \alpha_m \hat{z} \times \mathbf{v}_i = \mathbf{F}_i^{\text{obs}} + \mathbf{F}^{ac}. \quad (1)$$

Here α_d is the damping term which aligns the skyrmion velocity in the direction of the external forces, while α_m is the Magnus force which creates a velocity

component perpendicular to the forces on the skyrmion. We set $\alpha_d^2 + \alpha_m^2 = 1$. In the absence of pinning or obstacles and under a dc drive, the skyrmion would move at an angle known as the skyrmion Hall angle, $\theta_{sk} = \arctan(\alpha_m/\alpha_d)$

The force between an obstacle and the skyrmion is given by $\mathbf{F}_i^{\text{obs}} = -\nabla U_o = -F_o r_{io} e^{-(r_{io}/a_o)^2} \hat{\mathbf{r}}_{io}$, with $F_o = 2U_o/R_o^2$. The potential energy of the obstacle is $U_o = C_o e^{-(r_{io}/a_o)^2}$, where C_o is the strength of the obstacle potential, r_{io} is the distance between skyrmion i and obstacle o , and $R_o = R_o^L$ or R_o^S is the obstacle radius. We fix $R_o^L = 0.85$ and $R_o^S = 0.45$. For computational efficiency, we cut off the obstacle interaction beyond $r_{io} = 2.0$ since the interaction is negligible for larger distances. We set the obstacle density to $\rho_o = 0.093$ and use a total system size of 72×72 . The sample contains two different obstacle lattices which have the same lattice constant but different obstacle radii. In Fig. 1 we show an example in which the larger obstacles are embedded into a square region of the smaller obstacle lattice. We can also place one size of obstacle in each half of the sample to create a pair of one-dimensional (1D) interfaces, as in Fig. 2. The skyrmion couples to a biharmonic ac drive of the form $\mathbf{F}^{ac} = A \sin(\omega t) \hat{\mathbf{x}} + B \cos(\omega t) \hat{\mathbf{y}}$, where in this work we set $A = B$. The ac drive frequency ω is measured in inverse simulation time steps. We measure the normalized average skyrmion velocity in the x direction, $\langle V_x \rangle = \langle \mathbf{v}_i \cdot \hat{\mathbf{x}} \rangle / \omega a$, and in the y direction, $\langle V_y \rangle = \langle \mathbf{v}_i \cdot \hat{\mathbf{y}} \rangle / \omega a$. Under this normalization, a value of $\langle V_x \rangle = 1$ ($\langle V_y \rangle = 1$) indicates that the skyrmion is moving by one lattice constant in the x (y) direction during each ac drive cycle. We increase the ac drive amplitude A in small steps of $\delta A = 0.002$ and wait 10^5 simulation time steps between increments.

3. Transport Along a 1D Interface

We first consider a skyrmion interacting with a 1D interface as shown in Fig. 2. We can place the skyrmion within the middle of one of the obstacle lattices or along the interface. In Fig. 2, the small obstacles are in the upper portion of the sample, the large obstacles are in the lower portion of the sample, $\alpha_m/\alpha_d = 0.45$, and $\omega = 1 \times 10^{-5}$. If the skyrmion interacts with only one size of obstacle, it undergoes either localized motion or chaotic delocalized motion but shows little to no directed transport. When the skyrmion is placed near the interface for ac drive amplitude $A = 0.1$, as in Fig. 2(a), it moves in a periodic orbit around a single obstacle. If the particle is placed on the other side of the interface, it again forms a localized orbit which either circles one obstacle or follows a closed path between adjacent obstacles. If the drive amplitude is increased to $A = 0.4$, as in Fig. 2(b), the skyrmion follows a localized orbit that encircles four obstacles. Depending on the initial placement of the skyrmion, there can be an initial transient of chaotic motion, but the skyrmion quickly settles into a localized state for this value of A . It is also possible for the skyrmion to exhibit chaotic motion on one side of the interface but to settle into a localized orbit once it migrates to the other side of the interface. In Fig. 2(c) we show the formation of a translating orbit at $A = 0.5$ where the

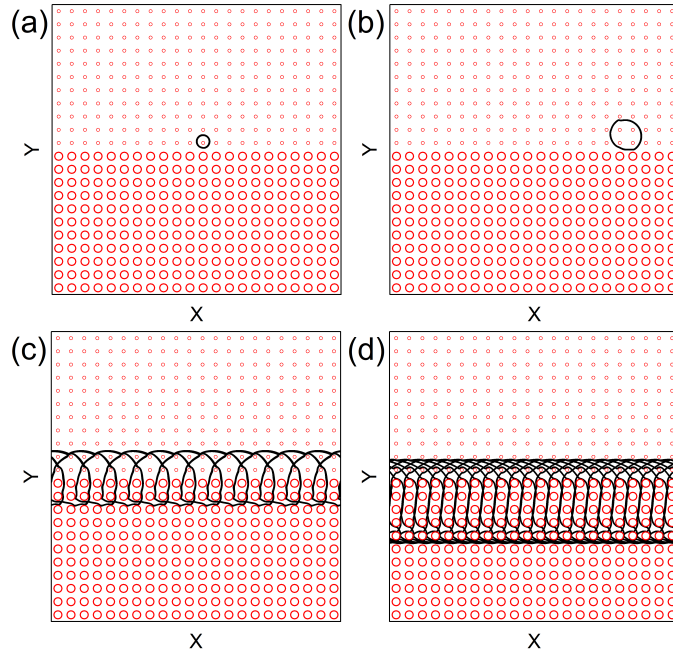


Figure 2: Obstacle locations (circles) and skyrmion trajectory (lines) in a system with a 1D interface between the large and small obstacles at $\alpha_m/\alpha_d = 0.45$ under a circular ac drive of frequency $\omega = 1 \times 10^{-5}$ and amplitude A . (a) At $A = 0.1$ the motion is localized. (b) A larger localized orbit at $A = 0.4$. (c) $A = 0.5$ where the skyrmion translates in the positive x -direction by $2a$ during every ac cycle. (d) At $A = 0.77$, there is another translating orbit where the skyrmion moves a distance a in the positive x direction every ac cycle.

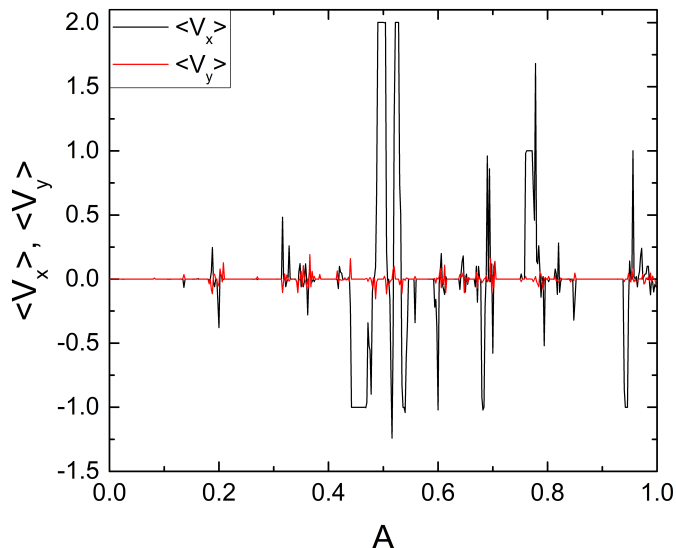


Figure 3: $\langle V_x \rangle$ (black) and $\langle V_y \rangle$ (red) vs A for the system in Fig. 2 with $\alpha_m/\alpha_d = 0.45$ and $\omega = 1 \times 10^{-5}$. Here there are several regions where $\langle V_x \rangle = \pm 1.0$ or 2.0 , indicating translating orbits.

skyrmion moves a distance $2a$ in the positive x direction during every ac drive cycle. Figure 2(d) illustrates another translating orbit at $A = 0.77$, where the skyrmion moves a distance a in the positive x -direction per ac drive cycle.

In Fig. 3 we plot $\langle V_x \rangle$ and $\langle V_y \rangle$ versus ac amplitude A for the system in Fig. 2. Here $\langle V_y \rangle \approx 0$ for all A since transport can occur only parallel to the interface, which is aligned in the x direction. The skyrmion can translate in either the positive or negative x direction. When $0.425 < A < 0.75$, the skyrmion moves along the interface a distance a in the negative x direction during each ac drive cycle, while for $0.475 < A < 0.51$, the skyrmion translates in the positive x direction by $2a$ during each cycle. There are also several other windows in which the skyrmion translates by a or $a/2$ in the positive or negative x direction. If the ac drive polarity is reversed, we obtain the same curves shown in Fig. 3 but with the y -axis flipped. The directed motion occurs along the interface due to a combination of the broken time symmetry from the ac drive and the broken spatial symmetry of the interface, which produces a ratchet effect. It was shown in previous work that when a particle is interacting with a periodic substrate, directed motion can occur in the absence of an interface if the ac drive itself breaks spatial symmetry, as can be achieved with biharmonic driving of mixed drive amplitude or frequency [42]. In the case we consider here, the ac driving is spatially symmetric, but when one portion of the skyrmion orbit is on one side of the interface and the other portion of the orbit is on the other side of the interface, the orbit becomes asymmetric and the ratchet effect can occur.

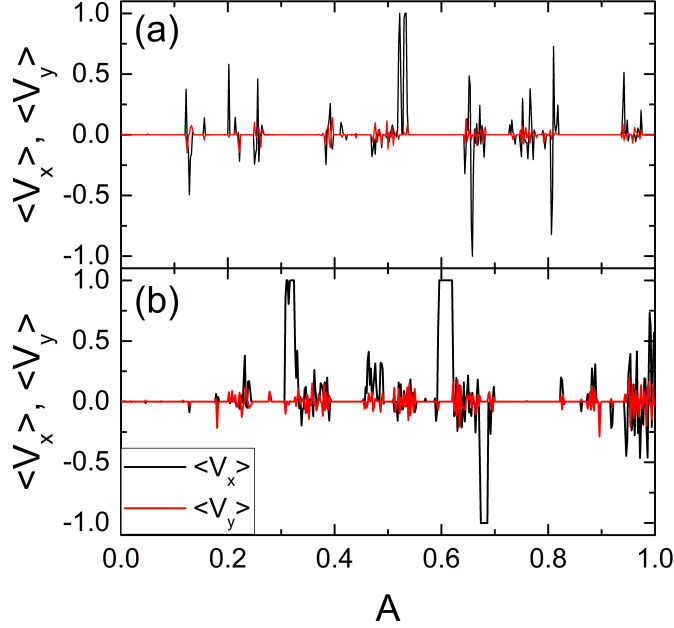


Figure 4: $\langle V_x \rangle$ (black) and $\langle V_y \rangle$ vs A for the system in Fig. 2 with $\omega = 1 \times 10^{-5}$. (a) $\alpha_m/\alpha_d = 1.732$. (b) $\alpha_m/\alpha_d = 9.962$, where extended windows of directed motion appear.

In Fig. 4 we plot $\langle V_x \rangle$ and $\langle V_y \rangle$ versus A for the same system as in Fig. 2 but with a stronger Magnus force component of $\alpha_m/\alpha_d = 1.732$ [Fig. 4(a)] or $\alpha_m/\alpha_d = 9.962$ [Fig. 4(b)]. For $\alpha_m/\alpha_d = 1.732$ in Fig. 4(a), there are some small regions of directed motion, while for $\alpha_m/\alpha_d = 9.962$ in Fig. 4(b), the directed motion regions are more extended. In Fig. 5(a) we illustrate the skyrmion trajectories for the system in Fig. 4(a) at $A = 0.22$, where the skyrmion starts at the edge of the interface and exhibits a short time transient translation in the small obstacle region before undergoing delocalized motion in the large obstacle region. In this case there is some translation in the positive x direction but the overall motion is a mixture of localized, chaotic and translating orbits. The skyrmion eventually becomes localized in the small obstacle region. Figure 5(b) shows the trajectory for the same system at $A = 0.534$, where the skyrmion forms a translating orbit moving a distance a in the positive x direction during each drive cycle. In Fig. 5(c) we plot a delocalized orbit for the system in Fig. 4(b) with $\alpha_m/\alpha_d = 9.862$ at $A = 0.382$, while Fig. 5(d) shows the same system at $A = 0.6$ where the skyrmion moves in a complex orbit at the edge of the interface that translates a distance a in the positive x direction during each ac cycle. In general, as α_m/α_d increases, the non-translating states take the form of chaotic or delocalized paths rather than closed localized orbits.

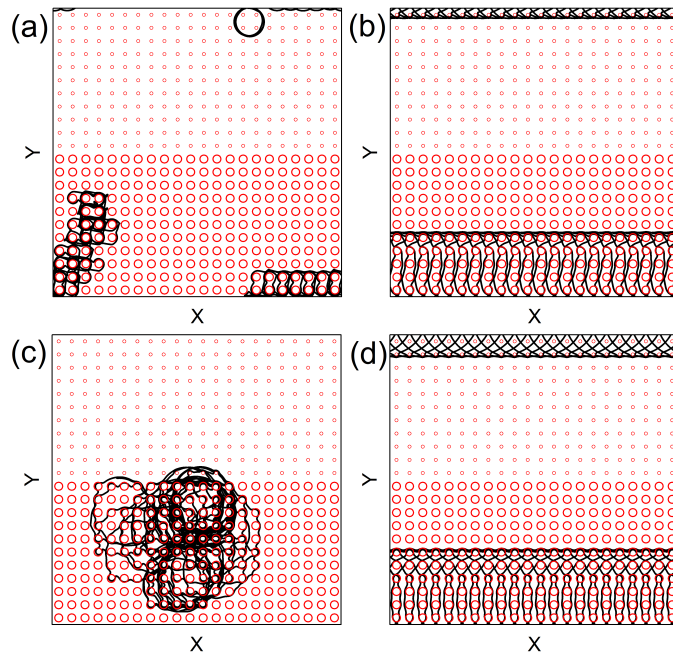


Figure 5: The obstacle locations (circles) and skyrmion trajectories (lines) for the system in Fig. 4 with $\omega = 1 \times 10^{-5}$. (a) At $\alpha_m/\alpha_d = 1.732$ and $A = 0.22$ there is a short time transient of directed motion before the skyrmion motion delocalizes. (b) A translating orbit at $\alpha_m/\alpha_d = 1.732$ and $A = 0.534$. (c) A delocalized orbit at $\alpha_m/\alpha_d = 9.962$ and $A = 0.372$. (d) A complex translating orbit at $\alpha_m/\alpha_d = 9.962$ and $A = 0.6$.

4. Guided Transport Along Corners

Now that we have established that skyrmions can undergo directed transport along a straight interface, the next question is whether the skyrmion can continue to follow an interface that changes direction or has a corner or even multiple corners. If so, it would be possible to guide a skyrmion along complex interface geometries in order to achieve various types of devices. To examine this question we consider the geometry illustrated in Fig. 1 where the large obstacles are placed in a square region in the center of the small obstacle lattice. In Fig. 6 we show some representative orbits for the system in Fig. 1 with $\alpha_m/\alpha_d = 0.45$ and $\omega = 1 \times 10^{-5}$. Localized orbits appear in Fig. 6(a) at $A = 0.1$ and in Fig. 6(b) at $A = 0.2$. A localized orbit forms in the small obstacle region at $A = 0.4$ in Fig. 6(c). At $A = 0.47$, a sample with a 1D interface has a translating orbit with motion in the positive x direction. In Fig. 6(d), the skyrmion is able to follow the interface at $A = 0.47$ and turn at all four corners, forming a large scale clockwise orbit along which the skyrmion moves by a distance $2a$ during every drive cycle. Figure 6(e) shows a localized orbit encircling 23 obstacles at $A = 0.66$. In Fig. 6(f) at $A = 0.86$, another large scale interface-following translating orbit appears which is wider than the orbit shown in Fig. 6(d).

In Fig. 7 we plot $\langle V_x \rangle$ and $\langle V_y \rangle$ for the system in Fig. 6. Unlike the case for motion along a 1D interface, there are now finite velocity components in both directions. Since the skyrmion is changing directions as it translates, the velocity components do not show the smooth steps found for the 1D interface motion; however, the regions where translation occurs are marked by large fluctuations or oscillations in $\langle V_x \rangle$ and $\langle V_y \rangle$. There are several intervals of A in which the skyrmion undergoes transport along the interface. There are also some intervals in which the skyrmion translates along straight portions of the interface but cannot turn a corner, so that the skyrmion motion becomes delocalized once the corner is passed.

In general, the values of α_m/α_d and A at which directed motion can occur along a 1D interface are the same as the values at which the skyrmion can move along an interface and turn a corner; however, the interval of A over which the corner-turning behavior appears is somewhat reduced compared to the interval in which 1D translation appears. We show an example of this in Fig. 8(a) at $A = 0.886$ for a system similar to that in Fig. 6 but for a higher frequency of $\omega = 2 \times 10^{-5}$. In this case, the skyrmion motion is chaotic in the region of small obstacles, but the skyrmion can follow the interface along a straight line. It cannot, however, turn the corner, so the motion becomes delocalized again once the skyrmion reaches the right edge of the large obstacle region. Figure 8(b) shows the same system at $A = 0.894$ where the skyrmion can now turn the corners. As A is increased, we find additional regimes in which the skyrmion can only move linearly along one side of the interface before returning to a delocalized or localized state after passing the corner of the large obstacle region.

For fixed ω , as α_m/α_d increases we find a regime in which the skyrmion can traverse the interface and turn corners yet has a partially stochastic component

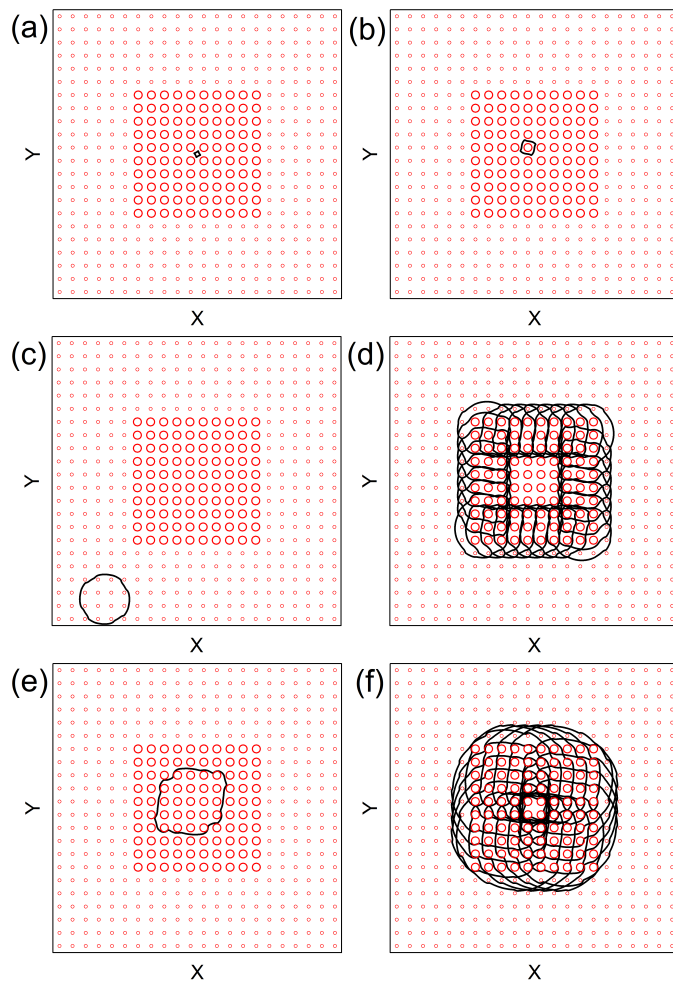


Figure 6: Obstacle locations (circles) and skyrmion trajectories (lines) for the system in Fig. 1 with $\alpha_m/\alpha_d = 0.45$ and $\omega = 1 \times 10^{-5}$. (a) A localized orbit at $A = 0.1$ which encircles no obstacles. (b) Another localized orbit at $A = 0.2$ which encircles a single obstacle. (c) A localized orbit at $A = 0.4$ in the small obstacle region which encircles 12 obstacles. (d) At $A = 0.47$, the skyrmion can translate along the interface and move around all four corners to form a large scale clockwise moving orbit. (e) At $A = 0.66$, the skyrmion is localized again. (f) At $A = 0.86$, another translating orbit appears.

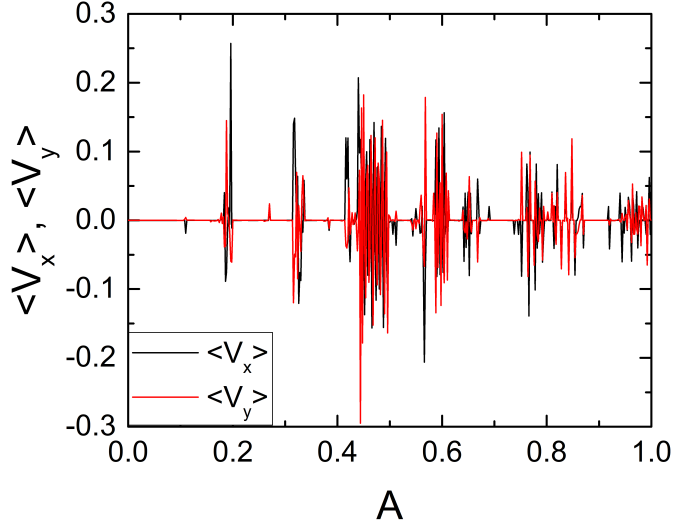


Figure 7: $\langle V_x \rangle$ (black) and $\langle V_y \rangle$ (red) vs A for the system in Fig. 6 with $\alpha_m/\alpha_d = 0.45$ and $\omega = 1 \times 10^{-5}$. The regions in which oscillations appear in $\langle V_x \rangle$ and $\langle V_y \rangle$ correspond to regions in which the skyrmion is translating around the interface.

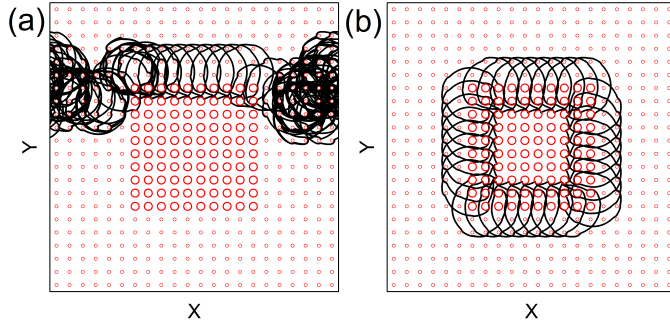


Figure 8: Obstacle locations (circles) and skyrmion trajectories (lines) for a system similar to that in Fig. 6 with $\alpha_m/\alpha_d = 0.45$ but at $\omega = 2 \times 10^{-5}$. (a) At $A = 0.886$, the skyrmion can translate linearly along the interface but cannot turn a corner. (b) At $A = 0.895$, the skyrmion can both translate and turn corners.

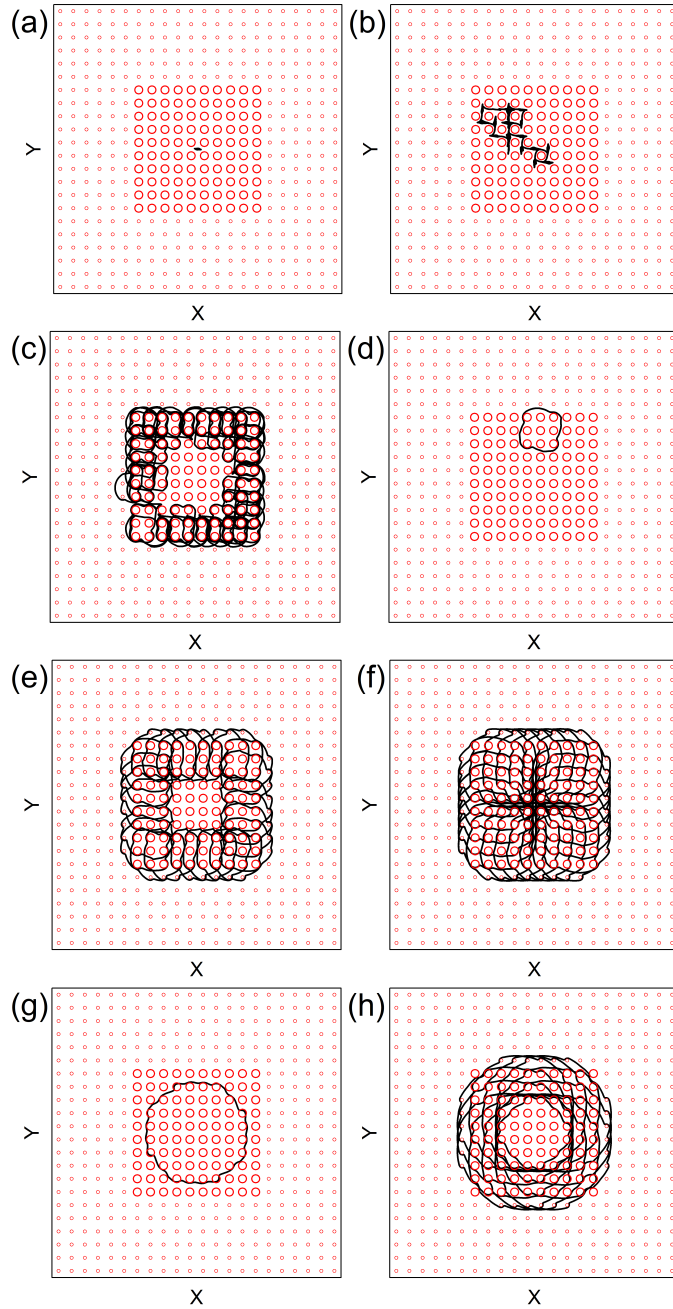


Figure 9: Obstacle locations (circles) and skyrmion orbits (lines) for a system with $\alpha_m/\alpha_d = 1.732$ and $\omega = 1 \times 10^{-5}$. (a) Localized motion at $A = 0.06$. (b) At $A = 0.074$, there is stochastic motion in the bulk but no translation. (c) At $A = 0.246$ there is interface motion with intermittent chaotic intervals. (d) A localized orbit at $A = 0.33$. (e) A translating orbit at $A = 0.38$. (f) A translating orbit at $A = 0.532$. (g) A localized orbit at $A = 0.74$. (h) A translating orbit at $A = 0.838$.

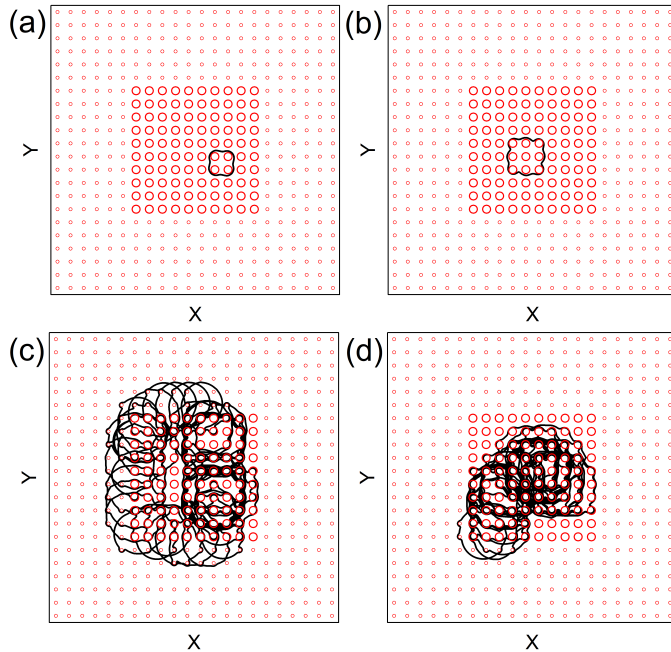


Figure 10: Obstacle locations (circles) and skyrmion orbits (lines) for a system with $\alpha_m/\alpha_d = 9.962$ and $\omega = 1 \times 10^{-5}$. (a) A localized orbit encircling four obstacles at $A = 0.03$. (b) A localized orbit encircling nine obstacles at $A = 0.1$. (c) At $A = 0.324$, the skyrmion jumps between chaotic motion in the bulk and translating motion along the interface. (d) At $A = 0.34$ there is chaotic motion in the bulk but no edge transport.

to its motion. In Fig. 9(a) we illustrate the localized orbit that forms for a system with $\alpha_m/\alpha_d = 1.732$ at $A = 0.06$. In the same system at $A = 0.074$, Fig. 9(b) shows that the skyrmion undergoes chaotic motion in the center bulk region but there is no directed motion. In Fig. 9(c) at $A = 0.246$, directed motion occurs along the interface but there are intermittent windows of chaotic motion, reducing the efficiency of the transport to a distance of much less than a per ac drive cycle. Figure 9(d) shows a localized orbit at $A = 0.33$. In Fig. 9(e), there is a strongly translating orbit at $A = 0.38$. Another translating orbit at $A = 0.532$ appears in Fig. 9(f). In Fig. 9(g) we illustrate a localized orbit at $A = 0.74$ that encircles 52 obstacles, while Fig. 9(h) shows another translating orbit at $A = 0.838$.

For even higher values of α_m/α_d , chaotic motion becomes more prevalent. In Fig. 10(a,b) we show the trajectories for a system similar to that in Fig. 9 but at $\alpha_m/\alpha_d = 9.962$ for $A = 0.03$ and $A = 0.1$. The orbits are localized and the skyrmion encircles four and nine obstacles, respectively. For larger A , chaotic motion in the bulk accompanies transport along the edges, as shown in Fig. 10(c) at $A = 0.324$. Here the skyrmion undergoes stochastic motion in the bulk but performs directed transport along half of the interface before reentering the bulk region and returning to a stochastic trajectory. For long

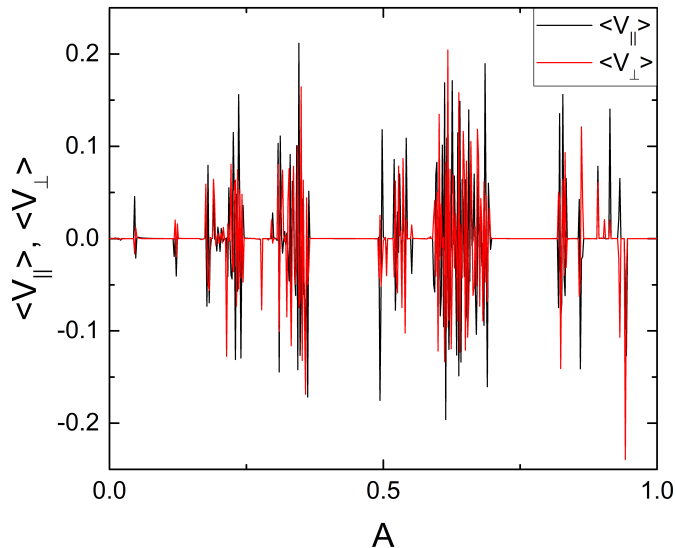


Figure 11: $\langle V_x \rangle$ (black) and $\langle V_y \rangle$ (red) vs A for the system in Fig. 10 with $\alpha_m/\alpha_d = 9.962$ and $\omega = 1 \times 10^{-5}$. Regions in which $\langle V_x \rangle$ and $\langle V_y \rangle$ are oscillating correspond to directed transport around the interface.

times this pattern repeats itself. In Fig. 10(d) we plot the trajectory at $A = 0.34$ where the motion is chaotic in the bulk but no edge transport occurs along the interface. In Fig. 11 we plot $\langle V_x \rangle$ and $\langle V_y \rangle$ versus A for the system in Fig. 10 showing that there are numerous regions where strong oscillations of the velocity appear, corresponding to intermittent transport along the interface or ordered motion in the bulk. There are several regions of localized motion in which $\langle V_x \rangle = \langle V_y \rangle = 0$.

5. Discussion

A recent study showed directed motion for particles interacting with a periodic lattice substrate in what are called colloidal topological insulators [41, 43]. Here, a colloid driven in a circular or closed orbit can exhibit directed transport when interacting with the interface between two different types of substrate lattices. Our results suggest that if a group of skyrmions is interacting with an interface in a substrate, various types of edge transport modes could occur that would create a version of a skyrmion topological insulator in which skyrmion motion would not occur in the bulk but could appear along the edge. Regarding possible collective effects, if the number of skyrmions is low we would expect behavior similar to that described in this work; however, if two or more skyrmions are close together, they could form a more complex orbit and move as a group along the edge. Since the number of degrees of freedom in such a translating object is higher, it is possible that a variety of fractional motions could occur

and that groups of skyrmions could form a composite skyrmion state. We have only considered the case in which the lattice constant is the same but the size of the obstacles is different in the two lattices. It would also be interesting to consider an interface between two different types of lattices, such as square and triangular, or between two lattices with different lattice constants. Our particle-based approach neglects the internal modes of the skyrmions, and has been shown to produce various types of ratchet effects for skyrmions interacting with asymmetric substrates [44, 45]. In continuum models which include skyrmion breathing modes, new types of ratchet effects can occur even in the absence of a substrate [46, 47]. This suggests that when internal modes are taken into account, there could be additional ways in which the skyrmion could translate along the interface, and that there could also be additional methods of driving the system such as with an oscillating magnetic field which could change the size or shape of the skyrmion as a function of time. There is also the question of thermal effects which could induce phase slips in the directed transport. Currently the closest geometry to the system we study is skyrmions interacting with antidot lattices such as those recently fabricated in Ref. [48]. Using this technique it would be possible to make a sample with a fixed substrate lattice constant but different antidot sizes in different regions.

6. Summary

We have examined skyrmion transport under circular ac driving along an interface between two different obstacle arrays which have the same lattice constant and different obstacle sizes. In the absence of an interface, there is no directed transport. Inclusion of the interface produces an additional spatial symmetry breaking that allows the skyrmion to translate along the interface due to a ratchet mechanism. As a result of the periodicity of the lattice, the skyrmion moves an integer or rational fractional number of lattice constants per ac drive cycle. In addition to linear transport along a 1D interface, we show that the skyrmion can turn corners in order to follow the interface and that motion in all four lattice symmetry directions can be induced with the same ac drive, suggesting that new types of skyrmion based devices could be created by having the skyrmion interact with interfaces. Our results are similar to the motion found for ac driven colloids in what are called colloidal topological insulators, where the colloids can undergo transport along the interface between two different types of substrate lattices.

CRedit authorship contribution statement

Nicolas Vizarim: Methodology, Investigation, Software, Visualization, Writing - Review & Editing. **Charles Reichhardt**: Conceptualization, Methodology, Writing - Original Draft. **Pablo Venegas**: Supervision, Funding acquisition. **Cynthia Reichhardt**: Software, Methodology, Writing - Review & Editing.

Declaration of Competing Interest

The authors declare that they have no known competing financial interests or personal relationships that could have appeared to influence the work reported in this paper.

Acknowledgement

This work was supported by the US Department of Energy through the Los Alamos National Laboratory. Los Alamos National Laboratory is operated by Triad National Security, LLC, for the National Nuclear Security Administration of the U. S. Department of Energy (Contract No. 892333218NCA000001). N.P.V. acknowledges funding from Fundação de Amparo à Pesquisa do Estado de São Paulo - FAPESP (Grant 2018/13198-7).

References

- [1] S. Mühlbauer, B. Binz, F. Jonietz, C. Pfleiderer, A. Rosch, A. Neubauer, R. Georgii, P. Böni, Skyrmion lattice in a chiral magnet, *Science* 323 (5916) (2009) 915–919. doi:10.1126/science.1166767.
- [2] X. Z. Yu, Y. Onose, N. Kanazawa, J. H. Park, J. H. Han, Y. Matsui, N. Nagaosa, Y. Tokura, Real-space observation of a two-dimensional skyrmion crystal, *Nature* (London) 465 (7300) (2010) 901–904. doi:10.1038/nature09124.
- [3] N. Nagaosa, Y. Tokura, Topological properties and dynamics of magnetic skyrmions, *Nature Nanotechnol.* 8 (12) (2013) 899–911. doi:10.1038/NNANO.2013.243.
- [4] K. Everschor-Sitte, J. Masell, R. M. Reeve, M. Kläui, Perspective: Magnetic skyrmions - Overview of recent progress in an active research field, *J. Appl. Phys.* 124 (24) (2018) 240901. doi:10.1063/1.5048972.
- [5] Y. Tokunaga, X. Z. Yu, J. S. White, H. M. Rønnow, D. Morikawa, Y. Taguchi, Y. Tokura, A new class of chiral materials hosting magnetic skyrmions beyond room temperature, *Nature Commun.* 6 (2015) 7638. doi:10.1038/ncomms8638.
- [6] S. Woo, K. Litzius, B. Krüger, M.-Y. Im, L. Caretta, K. Richter, M. Mann, A. Krone, R. M. Reeve, M. Weigand, P. Agrawal, I. Lemesch, M.-A. Mawass, P. Fischer, M. Kläui, G. S. D. Beach, Observation of room-temperature magnetic skyrmions and their current-driven dynamics in ultrathin metallic ferromagnets, *Nature Mater.* 15 (5) (2016) 501. doi:10.1038/NMAT4593.
- [7] A. Soumyanarayanan, M. Raju, A. L. G. Oyarce, A. K. C. Tan, M.-Y. Im, A. P. Petrovic, P. Ho, K. H. Khoo, M. Tran, C. K. Gan, F. Ernult, C. Panagopoulos, Tunable room-temperature magnetic skyrmions in Ir/Fe/Co/Pt multilayers, *Nature Mater.* 16 (9) (2017) 898. doi:10.1038/NMAT4934.

- [8] W. Legrand, D. Maccariello, N. Reyren, K. Garcia, C. Moutafis, C. Moreau-Luchaire, S. Coffin, K. Bouzehouane, V. Cros, A. Fert, Room-temperature current-induced generation and motion of sub-100 nm skyrmions, *Nano Lett.* 17 (4) (2017) 2703–2712. doi:10.1021/acs.nanolett.7b00649.
- [9] A. Fert, N. Reyren, V. Cros, Magnetic skyrmions: advances in physics and potential applications, *Nature Rev. Mater.* 2 (7) (2017) 17031. doi:10.1038/natrevmats.2017.31.
- [10] S. A. Montoya, R. Tolley, I. Gilbert, S.-G. Je, M.-Y. Im, E. E. Fullerton, Spin-orbit torque induced dipole skyrmion motion at room temperature, *Phys. Rev. B* 98 (2018) 104432. doi:10.1103/PhysRevB.98.104432.
- [11] A. Fert, V. Cros, J. Sampaio, Skyrmions on the track, *Nature Nanotechnol.* 8 (3) (2013) 152–156. doi:10.1038/nnano.2013.29.
- [12] R. Tomasello, E. Martinez, R. Zivieri, L. Torres, M. Carpentieri, G. Finocchio, A strategy for the design of skyrmion racetrack memories, *Sci. Rep.* 4 (2014) 6784. doi:10.1038/srep06784.
- [13] X. Zhang, M. Ezawa, Y. Zhou, Magnetic skyrmion logic gates: conversion, duplication and merging of skyrmions, *Sci. Rep* 5 (2015) 9400. doi:10.1038/srep09400.
- [14] D. Pinna, F. Abreu Araujo, J.-V. Kim, V. Cros, D. Querlioz, P. Bessiere, J. Droulez, J. Grollier, Skyrmion gas manipulation for probabilistic computing, *Phys. Rev. Applied* 9 (2018) 064018. doi:10.1103/PhysRevApplied.9.064018.
- [15] D. Prychynenko, M. Sitte, K. Litzius, B. Krüger, G. Bourianoff, M. Kläui, J. Sinova, K. Everschor-Sitte, Magnetic skyrmion as a nonlinear resistive element: A potential building block for reservoir computing, *Phys. Rev. Applied* 9 (2018) 014034. doi:10.1103/PhysRevApplied.9.014034.
- [16] K. M. Song, J.-S. Jeong, B. Pan, X. Zhang, J. Xia, S. Cha, T.-E. Park, K. Kim, S. Finizio, J. Raabe, J. Chang, J. Zhou, W. Zhao, W. Kang, H. Ju, S. Woo, Skyrmion-based artificial synapses for neuromorphic computing, *Nat. Electron.* 3 (2020) 148–155. doi:10.1038/s41928-020-0385-0.
- [17] F. Büttner, C. Moutafis, M. Schneider, B. Krüger, C. M. Günther, J. Geilhufe, C. v. K. Schmising, J. Mohanty, B. Pfau, S. Schaffert, A. Bisig, M. Förster, T. Schulz, C. A. F. Vaz, J. H. Franken, H. J. M. Swagten, M. Kläui, S. Eisebitt, Dynamics and inertia of skyrmionic spin structures, *Nature Phys.* 11 (3) (2015) 225–228. doi:10.1038/NPHYS3234.
- [18] B. L. Brown, U. C. Täuber, M. Pleimling, Effect of the Magnus force on skyrmion relaxation dynamics, *Phys. Rev. B* 97 (2018) 020405. doi:10.1103/PhysRevB.97.020405.

- [19] C. Reichhardt, D. Ray, C. J. O. Reichhardt, Collective transport properties of driven skyrmions with random disorder, *Phys. Rev. Lett.* 114 (2015) 217202. doi:10.1103/PhysRevLett.114.217202.
- [20] W. Jiang, X. Zhang, G. Yu, W. Zhang, X. Wang, M. B. Jungfleisch, J. E. Pearson, X. Cheng, O. Heinonen, K. L. Wang, Y. Zhou, A. Hoffmann, S. G. E. te Velthuis, Direct observation of the skyrmion Hall effect, *Nature Phys.* 13 (2) (2017) 162–169. doi:10.1038/NPHYS3883.
- [21] K. Litzius, I. Lemesh, B. Krüger, P. Bassirian, L. Caretta, K. Richter, F. Büttner, K. Sato, O. A. Tretiakov, J. Förster, R. M. Reeve, M. Weigand, L. Bykova, H. Stoll, G. Schütz, G. S. D. Beach, M. Kläui, Skyrmion Hall effect revealed by direct time-resolved X-ray microscopy, *Nature Phys.* 13 (2) (2017) 170–175. doi:10.1038/NPHYS4000.
- [22] S. Woo, K. M. Song, X. Zhang, Y. Zhou, M. Ezawa, X. Liu, S. Finizio, J. Raabe, N. J. Lee, S. Kim, S.-Y. Park, Y. Kim, J.-Y. Kim, D. Lee, O. Lee, J. W. Choi, B.-C. Min, H. C. Koo, J. Chang, Current-driven dynamics and inhibition of the skyrmion Hall effect of ferrimagnetic skyrmions in GdFeCo films, *Nature Commun.* 9 (2018) 959. doi:10.1038/s41467-018-03378-7.
- [23] C. Reichhardt, C. J. O. Reichhardt, Thermal creep and the skyrmion Hall angle in driven skyrmion crystals, *J. Phys.: Condens. Matter* 31 (7) (2019) 07LT01. doi:10.1088/1361-648X/aaefd7.
- [24] R. Juge, S.-G. Je, D. d. S. Chaves, L. D. Buda-Prejbeanu, J. Peña Garcia, J. Nath, I. M. Miron, K. G. Rana, L. Aballe, M. Foerster, F. Genuzio, T. O. Menteş, A. Locatelli, F. Maccherozzi, S. S. Dhesi, M. Belmeguenai, Y. Roussigné, S. Auffret, S. Pizzini, G. Gaudin, J. Vogel, O. Boulle, Current-driven skyrmion dynamics and drive-dependent skyrmion Hall effect in an ultrathin film, *Phys. Rev. Applied* 12 (2019) 044007. doi:10.1103/PhysRevApplied.12.044007.
- [25] K. Zeissler, S. Finizio, C. Barton, A. J. Huxtable, J. Massey, J. Raabe, A. V. Sadovnikov, S. A. Nikitov, R. Brearton, T. Hesjedal, G. van der Laan, M. C. Rosamond, E. H. Linfield, G. Burnell, C. H. Marrows, Diameter-independent skyrmion Hall angle observed in chiral magnetic multilayers, *Nature Commun.* 11 (1) (2020) 428. doi:10.1038/s41467-019-14232-9.
- [26] C. Reichhardt, C. J. O. Reichhardt, Shear banding, intermittency, jamming, and dynamic phases for skyrmions in inhomogeneous pinning arrays, *Phys. Rev. B* 101 (2020) 054423. doi:10.1103/PhysRevB.101.054423.
- [27] L. González-Gómez, J. Castell-Queralt, N. Del-Valle, A. Sanchez, C. Navau, Analytical modeling of the interaction between skyrmions and extended defects, *Phys. Rev. B* 100 (2019) 054440. doi:10.1103/PhysRevB.100.054440.

- [28] J. Castell-Queralt, L. González-Gómez, N. Del-Valle, C. Navau, Deterministic approach to skyrmionic dynamics at nonzero temperatures: Pinning sites and racetracks, *Phys. Rev. B* 101 (2020) 140404. doi:10.1103/PhysRevB.101.140404.
- [29] X. Zhang, G. P. Zhao, H. Fangohr, J. P. Liu, W. X. Xia, J. Xia, F. J. Morvan, Skyrmion-skyrmion and skyrmion-edge repulsions in skyrmion-based racetrack memory, *Sci. Rep.* 5 (2015) 7643. doi:10.1038/srep07643.
- [30] X. Xing, J. Åkerman, Y. Zhou, Enhanced skyrmion motion via strip domain wall, *Phys. Rev. B* 101 (2020) 214432. doi:10.1103/PhysRevB.101.214432.
- [31] C. Reichhardt, D. Ray, C. J. O. Reichhardt, Quantized transport for a skyrmion moving on a two-dimensional periodic substrate, *Phys. Rev. B* 91 (2015) 104426. doi:10.1103/PhysRevB.91.104426.
- [32] J. Feilhauer, S. Saha, J. Tobik, M. Zelent, L. J. Heyderman, M. Mruczkiewicz, Controlled motion of skyrmions in a magnetic antidot lattice [arXiv:arXiv:1910.07388](https://arxiv.org/abs/1910.07388).
- [33] N. P. Vizarim, C. Reichhardt, C. J. O. Reichhardt, P. A. Venegas, Skyrmion dynamics and topological sorting on periodic obstacle arrays, *New J. Phys.* 22 (2020) 053025. doi:10.1088/1367-2630/ab8045.
- [34] N. P. Vizarim, C. J. O. Reichhardt, P. A. Venegas, C. Reichhardt, Skyrmion dynamics and transverse mobility: skyrmion Hall angle reversal on 2D periodic substrates with dc and biharmonic ac drives, *Eur. Phys. J. B* 93 (2020) 112. doi:10.1140/epjb/e2020-10135-1.
- [35] N. P. Vizarim, C. Reichhardt, P. A. Venegas, C. J. O. Reichhardt, Shapiro steps and nonlinear skyrmion Hall angles for dc and ac driven skyrmions on a two dimensional periodic substrate, *Phys. Rev. B* (2020) (in press).
- [36] S. Shapiro, Josephson currents in superconducting tunneling: The effect of microwaves and other observations, *Phys. Rev. Lett.* 11 (1963) 80–82. doi:10.1103/PhysRevLett.11.80.
- [37] S. P. Benz, M. S. Rzchowski, M. Tinkham, C. J. Lobb, Fractional giant Shapiro steps and spatially correlated phase motion in 2D Josephson arrays, *Phys. Rev. Lett.* 64 (1990) 693–696. doi:10.1103/PhysRevLett.64.693.
- [38] L. Van Look, E. Rosseel, M. J. Van Bael, K. Temst, V. V. Moshchalkov, Y. Bruynseraede, Shapiro steps in a superconducting film with an antidot lattice, *Phys. Rev. B* 60 (1999) R6998–R7000. doi:10.1103/PhysRevB.60.R6998.
- [39] C. Reichhardt, R. T. Scalettar, G. T. Zimányi, N. Grønbech-Jensen, Phase-locking of vortex lattices interacting with periodic pinning, *Phys. Rev. B* 61 (2000) R11914–R11917. doi:10.1103/PhysRevB.61.R11914.

- [40] N. P. Vizarim, C. J. O. Reichhardt, P. A. Venegas, C. Reichhardt, Skyrmion pinball and directed motion on obstacle arrays, *J. Phys. Commun.* 4 (2020) 085001. doi:10.1088/2399-6528/aba9fb.
- [41] J. Loehr, D. de las Heras, A. Jarosz, M. Urbaniak, F. Stobiecki, A. Tomita, R. Huhnstock, I. Koch, A. Ehresmann, D. Holzinger, T. M. Fischer, Colloidal topological insulators, *Commun. Phys.* 1 (2018) 4. doi:10.1038/s42005-017-0004-1.
- [42] C. Reichhardt, C. J. Olson Reichhardt, Absolute transverse mobility and ratchet effect on periodic two-dimensional symmetric substrates, *Phys. Rev. E* 68 (2003) 046102. doi:10.1103/PhysRevE.68.046102.
- [43] H. Massana-Cid, A. Ernst, D. de las Heras, A. Jarosz, M. Urbaniak, F. Stobiecki, A. Tomita, R. Huhnstock, I. Koch, A. Ehresmann, D. Holzinger, T. M. Fischer, Edge transport at the boundary between topologically equivalent lattices, *Soft Matter* 15 (7) (2019) 1539-1550. doi:10.1039/c8sm02005a.
- [44] C. Reichhardt, D. Ray, C. J. O. Reichhardt, Magnus-induced ratchet effects for skyrmions interacting with asymmetric substrates, *New J. Phys.* 17 (2015) 073034. doi:10.1088/1367-2630/17/7/073034.
- [45] X. Ma, C. J. O. Reichhardt, C. Reichhardt, Reversible vector ratchets for skyrmion systems, *Phys. Rev. B* 95 (2017) 104401. doi:10.1103/PhysRevB.95.104401.
- [46] W. Chen, L. Liu, Y. Ji, Y. Zheng, Skyrmion ratchet effect driven by a biharmonic force, *Phys. Rev. B* 99 (2019) 064431. doi:10.1103/PhysRevB.99.064431.
- [47] W. Chen, L. Liu, Y. Zheng, Ultrafast ratchet dynamics of skyrmion by defect engineering under gigahertz magnetic fields [arXiv:arXiv:2002.08865](https://arxiv.org/abs/2002.08865).
- [48] S. Saha, M. Zelent, S. Finizio, M. Mruczkiewicz, S. Tacchi, A. K. Suszka, S. Wintz, N. S. Bingham, J. Raabe, M. Krawczyk, L. J. Heyderman, Formation of néel-type skyrmions in an antidot lattice with perpendicular magnetic anisotropy, *Phys. Rev. B* 100 (2019) 144435. doi:10.1103/PhysRevB.100.144435.